Science of the Total Environment 670 (2019) 1049–1059

Contents lists available at ScienceDirect

Science of the Total Environment

journal homepage: www.elsevier.com/locate/scitotenv

Estuarine salinity recovery from an extreme precipitation event: Hurricane Harvey in Galveston Bay

Jiabi Du *, Kyeong Park

Department of Marine Sciences, Texas A&M University at Galveston, Galveston, TX 77554, United States of America

HIGHLIGHTS

- The model reproduces well the dramatic response of Galveston Bay to Harvey.
- Salinity recovery time was two months on average with great spatial variability.
- Salinity recovery time responses non-linearly with the amount of stormwater input.
- Tidal pumping was the primary mechanism for salt influx through the bay entrance.
- Tidal pumping induced salt influx was facilitated by the shelf current.

GRAPHICAL ABSTRACT

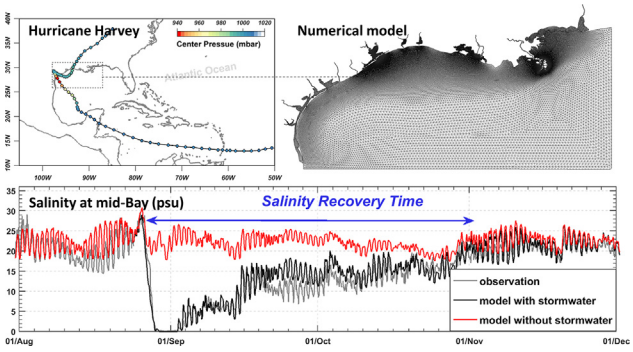

ARTICLE INFO

Article history:
Received 12 February 2019
Received in revised form 16 March 2019
Accepted 17 March 2019
Available online 19 March 2019

Editor: Damia Barcelo

Keywords:
Stormwater
Salt flux
Tidal pumping
Hydrodynamic model
Gulf of Mexico
SCHISM

ABSTRACT

With a warming climate and a more humid atmosphere, extreme precipitation events are projected to occur more frequently in future. Understanding how coastal systems respond to and recover from such acute events is of fundamental significance for environmental assessment and management. A hydrodynamic model was used to examine the estuarine responses in Galveston Bay to Hurricane Harvey, an extreme precipitation event with a return period of larger than 1000 years. The enormous freshwater input during Harvey caused long-lasting elevated water level, extraordinarily strong along-channel velocity, sharp decreases in salinity, and huge river plumes, all of which were well reproduced by the model. The salinity recovery time (T_R) was estimated as a measure of the system resiliency to stormwater input. Over the entire bay, the T_R had a mean of two months, but with great variability ranging from less than 10 days near the bay entrance to over three months in the inner part of Trinity Bay and the middle of East Bay. The spatially varying T_R was explained by different contributions of exchange flow and tidal pumping to salt flux. At the bay entrance, tidal pumping facilitated by the shelf current was the dominant mechanism for salt influx, while exchange flow and tidal pumping had a comparable contribution to salt influx to Trinity Bay. The spatial pattern of the T_R appears consistent with the changes in the phytoplankton community in the bay. A series of numerical experiments with different amounts of stormwater reveals a non-linear relationship between the bay-wide mean T_R and the amount of stormwater, with the rate of increase in T_R decreasing when stormwater input increases. The present approach using a hydrodynamic model will be able to provide a quick assessment of the environmental pressure from extreme events.

* Corresponding author.
E-mail address: jdu@tamug.edu (J. Du).

https://doi.org/10.1016/j.scitotenv.2019.03.265

1. Introduction

Extreme precipitation is projected to occur more frequently under the warming climate (Knight and Davis, 2009; Donat et al., 2016; Pfahl et al., 2017). Extreme precipitations, along with other types of extreme events (e.g., drought and heat wave), are posing increasing threats and pressure to ecosystems (Knapp et al., 2008), particularly in coastal areas (Weyhenmeyer et al., 2004; Cardoso et al., 2008). Large quantity of freshwater and sediment, resulting from extreme precipitation events, have great potential to renew estuarine water (Hagy et al., 2006), decrease salinity drastically (Du et al., 2019a), enhance turbidity (Zhang et al., 2013), bury benthic fauna (Posey et al., 1996), and shift plankton community (Scheffer et al., 2001; Peierls et al., 2003; Liu et al., 2019). The influence can be beneficial or detrimental, and the recovery from the acute perturbation may last for days, months, or even years, depending on the resiliency of the coastal system (Paerl et al., 2006). Many estuarine species such as plankton, fish, and seagrass have a certain range of salinity tolerance and can be stressed under too low or too high salinities. For instance, prolonged exposure to low-salinity condition can lead to enhanced mortality of eastern oyster (Munroe et al., 2013; Casas et al., 2018). Understanding the salinity recovery process is therefore of fundamental importance. Hurricane Harvey (2017), one of the most devastating hurricanes that hit the U.S. in recent history, brought enormous precipitation over the Texas-Louisiana coast, serving as a great example to examine the estuarine response to an extreme precipitation event, particularly in terms of salinity recovery.

Hurricane Harvey (hereinafter referred to as Harvey) intensified quickly in the northern Gulf of Mexico before making landfall on August 26, 2017 along the mid-Texas coast as a Category 4 hurricane (Fig. 1). Harvey brought record-breaking precipitation, with the return period of the peak 3-day precipitation exceeding 1000 years (van Oldenborgh et al., 2018), and caused more than 80 fatalities and over $150 billion economic losses, mostly due to the extraordinary flooding (Emanuel, 2017; Balaguru et al., 2018). Over the 5-day period from August 26 to 30, Harvey dumped 92.7×10^9 m^3 of water across Texas and Louisiana (Fritz and Samenow, 2017), making it the wettest tropical cyclone in the U.S. history. The extraordinary amount of water load even caused up to 21 mm subsidence of Earth's crust (Milliner et al., 2018). A freshwater load of 11.1×10^9 m^3 was estimated to discharge into Galveston Bay (about 3 times the bay volume), making the entire bay virtually fresh for several days (Du et al., 2019a). Due to the limited coverage of monitoring stations inside the bay, however, the speed and controlling mechanism(s) of salinity recovery are still not clearly understood. Furthermore, large sea-surface slope due to input of huge freshwater and mixing due to strong wind greatly disturbed the circulation inside and outside of the bay, making the salt exchange between the estuary and coastal ocean very different from that under normal conditions.

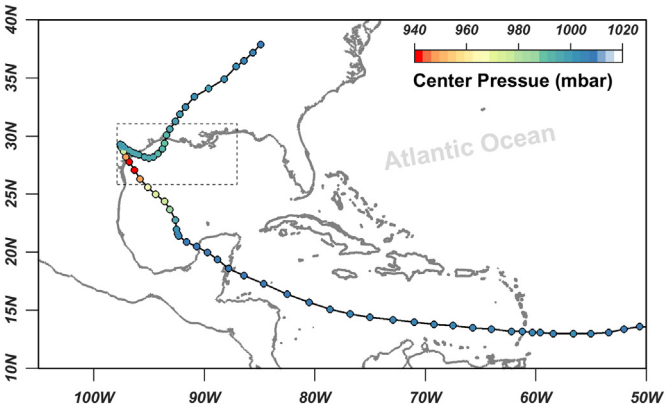

Fig. 1. Track of Hurricane Harvey from the National Hurricane Center (https://www.nhc.noaa.gov/data/hurdat/hurdat2-1851-2017-050118.txt, accessed on March 10, 2019), the center pressure (dot color), and the numerical model domain (rectangle).

Numerical models have been used to simulate storm conditions. Munroe et al. (2013) applied a model to study the effect on salinity in Delaware Bay of Hurricane Irene and Tropical Storm Lee (2011), which combined to dump 50% of the average annual cumulative precipitation into the watershed, and suggested a linkage between the prolonged low-salinity exposure and oyster mortality rate. Gong et al. (2007) applied a model to investigate the effect of Hurricane Isabel (2003) on the changes of stratification, salt flux, and the recovery time for the York River estuary. Numerical simulations of extreme precipitation events that make the entire estuary completely fresh are, however, rarely reported. In this study, we applied a hydrodynamic model to examine the salinity recovery in Galveston Bay after Harvey by calculating a timescale, "salinity recovery time" (T_R). We found large spatial variability of T_R in Galveston Bay and identified the underlying mechanisms responsible for the spatial heterogeneity. The timescale introduced and the methods used in this study shall be applicable to any estuary, serving as an efficient diagnostic tool for environmental assessment and management.

2. Methods

We employed the Semi-implicit Cross-scale Hydroscience Integrated System Model (SCHISM: Zhang et al., 2015, 2016), an open-source community-supported modeling system based on unstructured grids, derived from the early SELFE model (Zhang and Baptista, 2008). The model is based on the turbulence-averaged Navier-Stokes equations, including continuity, momentum, salt-balance, and heat-balance equations, under the hydrostatic approximation. It uses a semi-implicit Galerkin finite-element method for momentum advection and a finite-volume method for the mass advection. It uses the generic length-scale model of Umlauf and Burchard (2003) with the stability function of Kantha and Clayson (1994) for turbulence closure. The model has the capability of employing a very flexible vertical grid system, robustly and faithfully resolving the complex topography in estuarine and oceanic systems without any smoothing (Du et al., 2018a; Ye et al., 2018). A more detailed description of the SCHISM, including the governing equations, horizontal and vertical grids, numerical solution methods, and boundary conditions, can be found in Zhang et al. (2015, 2016).

The model domain (Fig. 2a) covers the entire Texas, Louisiana, Mississippi, and Alabama coasts, including the shelf as well as major estuaries (e.g., Galveston Bay), which allows to simulate the interactions between Galveston Bay and the shelf ocean that are critically important for salt and water exchange (Du et al., 2019b). The grid system contains 142,972 horizontal elements, with the resolution ranging from 40 m in the narrow ship channel of Galveston Bay to 10 km in the open ocean. The fine grid for the ship channel (Fig. 2b, c) is aligned with the channel orientation in order to accurately simulate the salt intrusion process (Ye et al., 2018). Vertically, a hybrid *s*-*z* grid is used, with 10 sigma layers for depths <20 m and another 30 *z*-layers for depths from 20 to 4000 m. The bathymetry used in the model is based on the coastal relief model (3 arc-second resolution: https://www.ngdc.noaa.gov). The local bathymetry in Galveston Bay is augmented by 10-m resolution DEM (digital elevation model) bathymetric data (https://catalog.data.gov/dataset/galveston-texas-coastal-digital-elevation-model) to resolve the narrow ship channel (150 m wide, 10–15 m deep) that extends from the bay entrance all the way to Port of Houston. When forced by realistic boundary conditions, including the open boundary conditions from FES2014 global tide (Carrere et al., 2015) and global HYCOM model output (https://www.hycom.org/data/glbu0pt08), atmospheric forcing from the European Centre for Medium-Range Weather Forecasts (ECMWF: https://www.ecmwf.int), and river discharges from 15 USGS gaging stations, the model gives a very good reproduction of the observed hydrodynamic conditions in 2007–2008 inside the Galveston Bay and over the

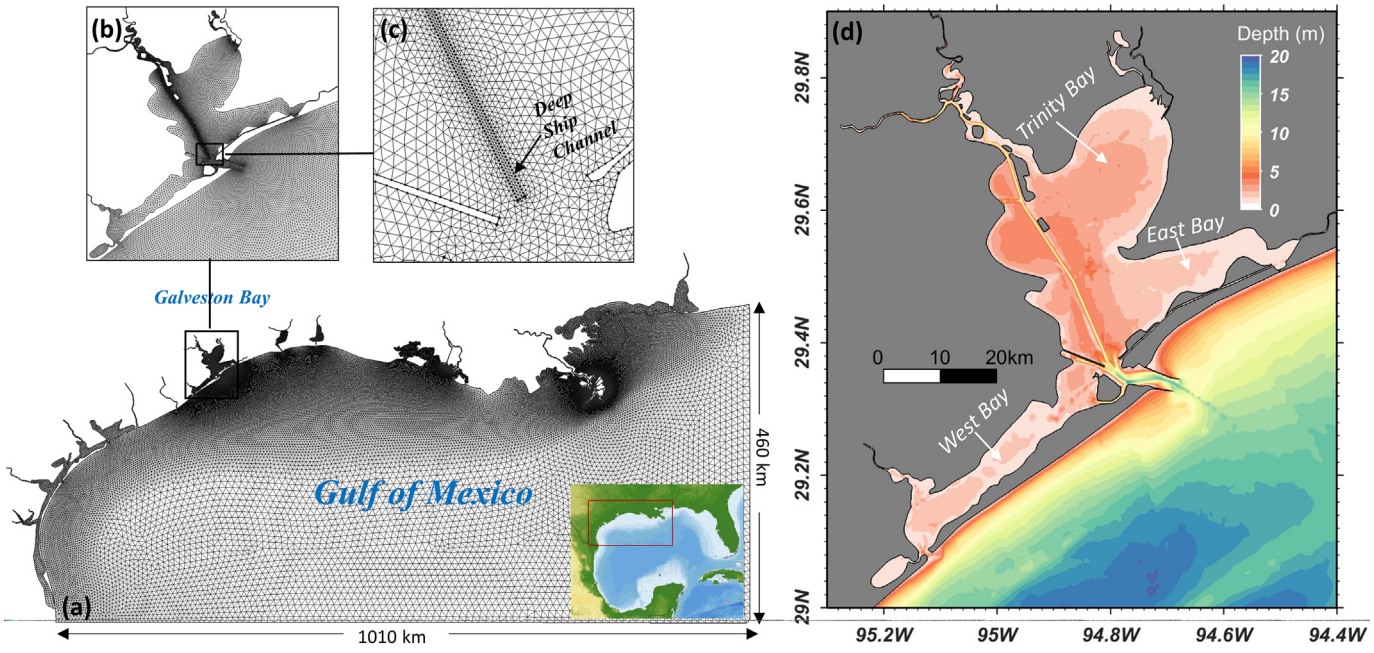

Fig. 2. The model domain with the horizontal grid (a), zoom-ins for the Galveston Bay (b) and its narrow, deep ship channel (c), and the bathymetry of Galveston Bay (d).

Texas- Louisiana shelf in terms of water level, salinity, temperature, stratification, and shelf current. A more detailed description of the model configuration, including the grid system, bathymetry, boundary conditions, and the 2007–2008 model validation results can be found in Du et al. (2019b).

We applied this model for the simulation of Harvey. For hurricane simulations, it is essential to ensure the credibility of the wind field as well as the freshwater load used for forcing conditions. The wind field was extracted from the ECMWF, which agrees well with the data for the hurricane track and location of hurricane eye from the National Hurricane Center (Fig. 3). It also agrees well with another independent data for hourly wind speed and direction from the NOAA station at the bay entrance (Fig. A1). For the freshwater input, it is important to note that Galveston Bay received not only freshwater from major rivers but

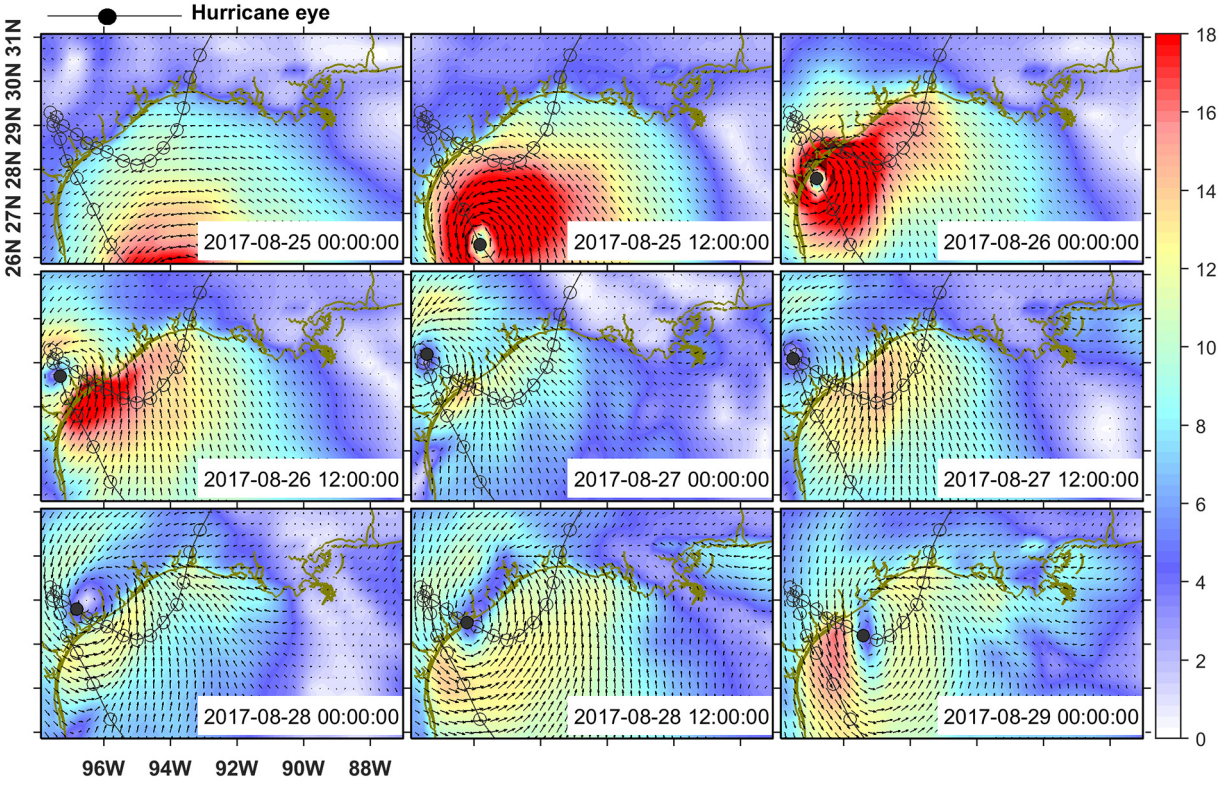

Fig. 3. Wind field from the European Centre for Medium-Range Weather Forecasts (ECMWF) and the hurricane track from the National Hurricane Center. The filled color denotes the wind speed ($m\,s^{-1}$) at 10 m above ground and the open circles denote the hurricane track with the black solid circle indicating the hurricane eye for the given time. Note the high consistency in the location of hurricane eye between two independent datasets.

also an enormous amount of freshwater through surface runoff and groundwater along the bay's coastline. Du et al. (2019a) estimated that 11.1×10^9 m^3 of freshwater entered the bay during Harvey, and 34% of it was through surface runoff and groundwater along the coastline. To account for this input, 65 point sources evenly distributed along the bay's coastline were considered (Fig. 4d). The daily discharge along the coastline was estimated by distributing the total coastline load (3.73×10^9 m^3) in proportion to the daily precipitation (Fig. 4c) and allocating the coastline load evenly to the 65 point source locations.

This method of accounting for the freshwater input through surface runoff and groundwater is not perfect. There was likely a delay between the time of precipitation and the time surface runoff and groundwater reached the bay, which would introduce errors when estimating the daily discharge in proportion to the daily precipitation. Allocating the total coastline load evenly to the 65 point source locations is also subject to uncertainties since the spatial allocation shall depend on the spatial distribution of precipitation and land use/land cover of the watershed. A better way would be to apply a watershed model to estimate the freshwater input through surface runoff and groundwater. However, most of the freshwater input along the coastline occurred on August 24–31, 2017 (Fig. 4c) while the main focus of this study is the salinity recover after Harvey, which was associated with a much longer timescale on the order of months (Fig. 5b). The bay received an enormous amount of freshwater, about 3 times the bay volume, which made the entire bay virtually fresh (Du et al., 2019a). Hence, a more accurate estimate of the freshwater input along the coastline may affect the progression of the bay water becoming fresh but is not likely to alter the post-storm process of salinity recovery. Furthermore, the model reproduces well not only the recovery of salinity in September and October but also the sudden drop in salinity to zero during Harvey (Fig. 5), providing confidence in the method of allocating the freshwater input along the coastline.

To examine the estuarine recovery from the impact of the Harvey's stormwater ΔQ (the freshwater load due to Harvey, defined as the difference between the discharge during Harvey and the pre-storm condition: see Fig. 4a–c), a numerical experiment without ΔQ was conducted. From the difference between two model runs with and without ΔQ, the salinity recovery time (T_R) for Harvey was estimated as the time for salinity values from the two model runs to converge (Fig. 5b). This definition is more robust compared to conventional methods that determine the recovery time as the time for salinity to recover to its pre-storm condition (e.g., Walker, 2001; Frazer et al., 2006). As the forcing conditions in an estuary, the adjacent shelf, and the atmosphere would not be the same before and after a storm, using the pre-storm condition as a reference will not be able to take into account the natural variability in salinity (Gong et al., 2007). We then conducted six additional numerical experiments with 10%, 20%, 30%, 40%, 50%, and 200% of ΔQ and estimated the corresponding T_R to further investigate the system's response to different amounts of stormwater input. The extraordinary Harvey's stormwater (ΔQ) is rare, with the return period exceeding 1000 years (van Oldenborgh et al., 2018), but precipitation events with smaller intensities (e.g., 10%–50% of ΔQ) are likely to occur more frequently. The results from numerical experiments were used to examine the relationship between T_R and stormwater input.

3. Results

3.1. Model-observation comparison: influence of stormwater

The model with the Harvey's stormwater ΔQ reproduces well the notable estuarine responses to Harvey. The subtidal water level is well simulated by the model (Fig. 6a). Typical storm surges mainly caused by wind generally last for one or two days (e.g., Valle-Levinson et al., 2002; Li et al., 2006; Shen et al., 2006; Rego and Li, 2010; Sebastian et al., 2014). During Harvey, however, the water level elevated by >1 m lasted over 6 days, which would not have been possible without ΔQ. Enormous freshwater input caused the water level 0.4–0.5 m higher in the middle and upper bay relative to the bay entrance (see Fig. 5a in Du et al., 2019a). The resulting surface slope generated strong along-channel velocity with the seaward speed exceeding 3 m s^{-1} at the buoy station in the lower reach of the San Jacinto River estuary, which was also reproduced well by the model with ΔQ (Fig. 6b). The model reproduces the tidal (astronomical) variation in velocity before and after Harvey, but it fails to reproduce the tidal variation that persisted on August 26–28. It should be noted that this discrepancy in velocity at the beginning of Harvey would not affect the model's credibility in simulating the salinity recovery after Harvey, the main topic of this study. Salinity decreased sharply throughout the bay and the entire bay became virtually fresh during Harvey, and it took months for salinity to return to pre-storm conditions, which the model also reproduces very well (Fig. 5).

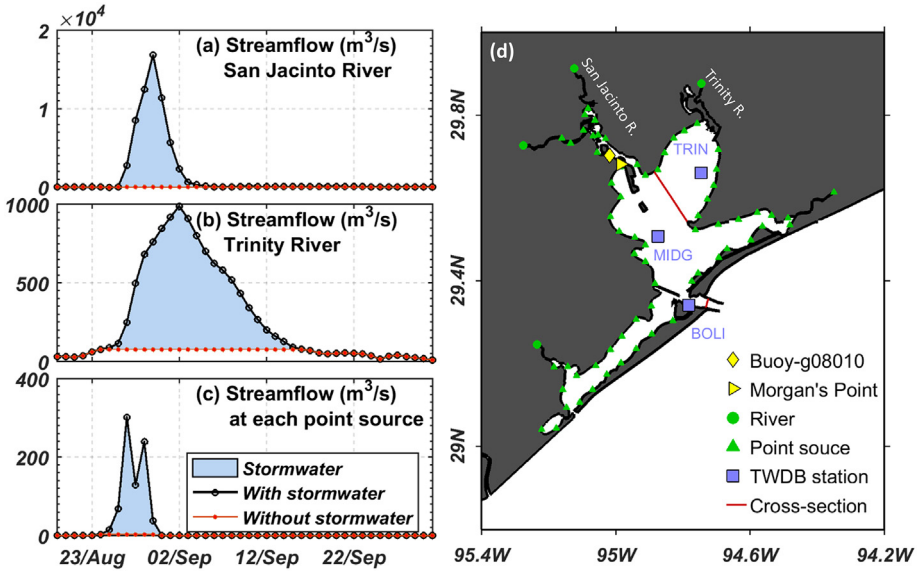

Fig. 4. River discharge from two major rivers, San Jacinto River (a) and Trinity River (b), and the estimated coastline freshwater load (c) at each of 65 point sources (d). The blue shade in (a)–(c) denotes the Harvey's stormwater ΔQ (the freshwater load due to Harvey, defined as the difference between the discharge during Harvey and the pre-storm condition). Also shown in (d) are the locations of major river input, monitoring stations for salinity, water level, and velocity, and two cross-sections (one across the bay entrance and the other across the mouth of Trinity Bay).

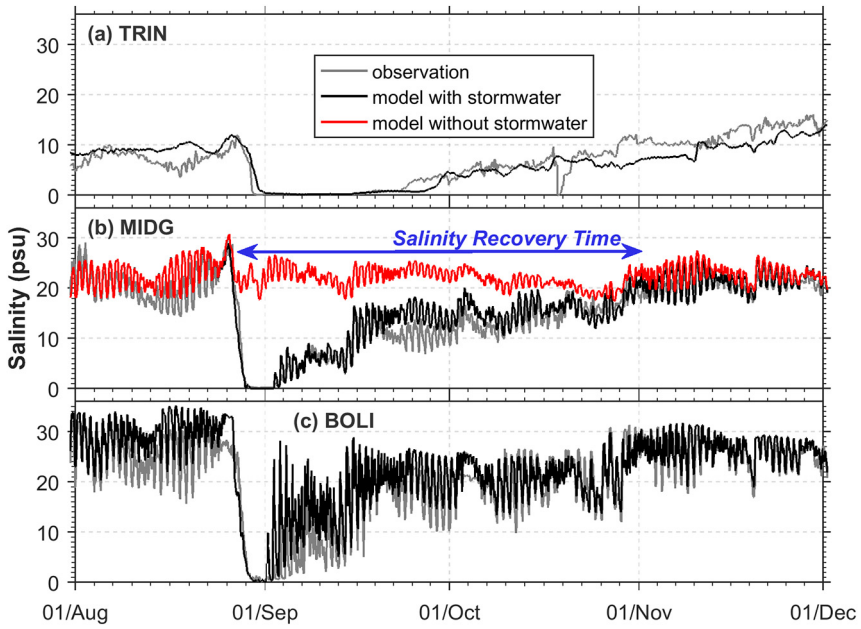

Fig. 5. The model-observation comparison for salinity at three TWDB (Texas Water Development Board) monitoring stations (see Fig. 4d for their locations). In (b), the red line shows the model result without the Harvey's stormwater, and the double arrow indicates the salinity recovery time (T_R).

Five metrics, the model skill (*Skill*: Willmott, 1981) and Nash–Sutcliffe model efficiency index (NSE: Nash and Sutcliffe, 1970) as well as the coefficient of determination (R^2), root mean square error (*RMSE*), and mean absolute error (*MAE*), were examined for quantitative assessment of the model performance:

$$Skill = 1 - \frac{\sum_{i=1}^{N} |M_i - O_i|^2}{\sum_{i=1}^{N} \left(|M_i - \overline{O}| + |O_i - \overline{O}| \right)^2} \quad (1)$$

$$NSE = 1 - \frac{\sum_{i=1}^{N} (M_i - O_i)^2}{\sum_{i=1}^{N} \left(O_i - \overline{O} \right)^2} \quad (2)$$

where O_i and M_i are the observed and modeled variables, respectively, with the overbar indicating the temporal average over the number of observations (N). *Skill*, ranging from 0 to 1, provides an index of model-data agreement, with a *skill* of 1 indicating perfect agreement and a *skill* of 0 indicating complete disagreement. *NSE* is a normalized

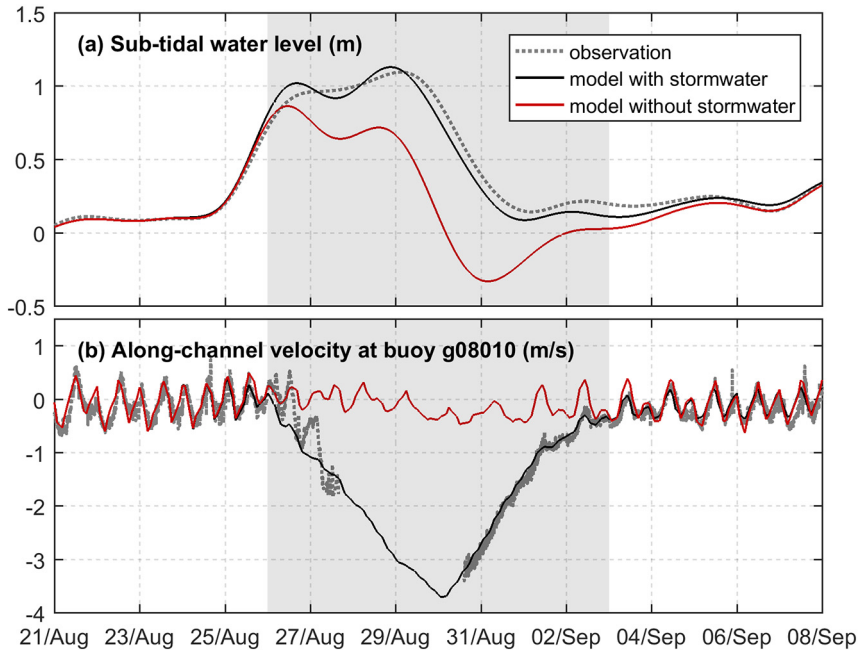

Fig. 6. The model-observation comparison for subtidal water level (m) at Morgan's Point (a) and along channel velocity (m s^{-1}) at buoy g080101 (b) (see Fig. 4d for their locations). The grey shades indicate the period of intense stormwater input from August 26 to September 3, 2017 based on the freshwater load from San Jacinto River in Fig. 4a.

statistic that indicates how well the plot of the data vs. model fits the 1:1 line. *NSE* can have values ≤1, with values between 0.50 and 0.65 considered as threshold values to indicate a model of sufficient quality (Moriasi et al., 2007; Ritter and Muñoz-Carpena, 2013). R^2 indicates the portion of the variance in the observed data explained by the model. R^2 ranges from 0 to 1, and typically values >0.5 are considered acceptable (Moriasi et al., 2007). The magnitude of *RMSE* and *MAE* indicates the average deviation between model and data.

These five metrics calculated for subtidal water level, along-channel velocity, and salinity suggest a satisfactory model performance for the 10-day period during Harvey as well as over the entire simulation period (Table 1). For salinity, in particular, *Skills* > 0.85, *NSEs* > 0.73, R^2 > 0.79, and *RMSEs* and *MAEs* are small relative to the observed ranges for the entire simulation period. The model performance is even better for the 10-day period during Harvey when dramatic changes in hydrodynamic conditions took place. The model also simulates well the overall shape, direction, and offshore extent of huge river plumes (Fig. 7). The good agreement between model and observation provides credibility of the model as well as the forcing conditions including wind and freshwater input.

3.2. Salinity recovery time (T_R)

The mean T_R averaged over the entire bay was about 62 days. The T_R exhibits great spatial variability and ranges from 6 to 108 days, with the smallest values (<10 days) at and near the three outlets, increasing values of up to about 60 days when moving upstream, and even larger values inside Trinity Bay where a maximum of >90 days was obtained in the bay's inner part (Fig. 8f). T_R is symmetric around the ship channel, and it increases when moving away from the channel. The tongue-shaped distribution of T_R is mainly attributable to the stronger salt intrusion along the deep ship channel (Du et al., 2018b). The strength of gravitational circulation, a typical two-layer circulation in an estuary with a landward bottom inflow driven by density gradient and a seaward surface outflow driven by surface slope, is proportional to water depth (MacCready and Geyer, 2010) and the stronger circulation along the deep channel tends to move the bottom higher salinity water faster to the upper estuary. Moreover, the differential longitudinal advection of saline water during flood tide, characterized by stronger flood current at deep channel than at shallow shoal (Huzzey and Brubaker, 1988), also contributes to the strong salt intrusion in deep ship channel (Lerczak and Geyer, 2004). Interestingly, the salinity recovery was very different between West Bay and East Bay, with much larger T_R in East Bay, even though the two bays share similar shape and bathymetry and have a similar distance relative to the main bay entrance. The much smaller T_R in West Bay can be attributed to the relatively wide outlet, San Luis Pass (1 km wide), relative to East Bay with a narrow outlet, Rollover Pass (52 m wide).

A series of numerical experiments with different amount of stormwater consistently shows that the lower part of the bay near the mouth is associated with the shortest T_R while the inner part of Trinity Bay and the middle of East Bay are associated with the longest T_R (Fig. 8). The bay-wide mean T_R exhibits a non-linear relationship with the amount of stormwater (Fig. 8h). The mean T_R increases rapidly and almost linearly with increasing stormwater from 10% to 30% of the Harvey's stormwater ΔQ, beyond which the rate of increase in the mean T_R reduces considerably. Once the bay becomes fresh with large stormwater, further increases in stormwater cannot make the bay fresher. However, larger stormwater input will always lower the salinity in the adjacent coastal sea, resulting in fresher ocean water (Fig. A2) and thus longer salinity recovery time. This relationship allows us to estimate the salinity recovery time for Galveston Bay once the stormwater amount is known.

Table 1
Metrics for model-observation comparison for the subtidal water level at Morgan's Point, along-channel velocity at buoy g08010, and salinity at three TWDB stations (see Fig. 4d for the station locations) over the entire simulation period and the 10-day period during Hurricane Harvey.

Comparison period	Variable	*Skill*	*NSE*	R^2	*RMSE*	*MAE*
Simulation period (7/1–12/31/2017)	Subtidal water level	0.98	0.91	0.92	0.07 m	0.04 m
	Along-channel velocity	0.94	0.78	0.79	0.16 m s^{-1}	0.13 m s^{-1}
	Salinity at TRIN	0.85	0.77	0.84	3.5 psu	2.4 psu
	Salinity at MIDG	0.94	0.73	0.83	3.0 psu	2.2 psu
	Salinity at BOLI	0.93	0.75	0.80	3.6 psu	2.7 psu
During Harvey (8/25–9/4/2017)	Subtidal water level	0.99	0.96	0.98	0.07 m	0.07 m
	Along-channel velocity	0.98	0.94	0.94	0.23 m s^{-1}	0.15 m s^{-1}
	Salinity at TRIN	0.96	0.85	0.93	1.8 psu	1.4 psu
	Salinity at MIDG	0.99	0.95	0.96	2.3 psu	1.4 psu
	Salinity at BOLI	0.96	0.83	0.87	4.6 psu	3.3 psu

4. Discussion

4.1. Mechanisms for salinity recovery

Salt mass inside an estuary, and thus salinity, is determined by the competition of salt influx and outflux. For steady state, the two opposing salt fluxes are balanced, resulting in constant salinities inside the estuary at subtidal timescales. The salinity recovery is controlled by the magnitude of salt influx. To understand the salt mass exchange between ocean and estuary and between the main bay and the sub-bay, the salt fluxes through the bay entrance cross-section and another cross-section that separates Trinity Bay from Galveston Bay were calculated (see Fig. 4d for their locations). By decomposing the normal velocity u and salinity S into tidally and cross-sectionally averaged (u_o and S_o), tidally averaged and cross-sectionally varying (u_e and S_e), and tidally and cross-sectionally varying (u_t and S_t) components, the contributions on salt flux (F_s) from three different mechanisms can be determined (Lerczak et al., 2006):

$$\begin{aligned} F_s &= \left\langle \int uSdA \right\rangle = \left\langle \int (u_o + u_e + u_t)(S_o + S_e + S_t)dA \right\rangle \\ &\approx \left\langle \int (u_o S_o + u_e S_e + u_t S_t)dA \right\rangle \equiv -Q_f S_o + F_e + F_t \end{aligned} \tag{3}$$

where A is the time-varying cross-sectional area; the angled bracket denotes tidal average; and Q_f is the subtidal volume discharge rate. The three terms on the right-hand side of Eq. (3) represent the subtidal salt flux due to cross-sectional average advective transport ($-Q_f S_o$), shear dispersion due to vertical and lateral shear transport (F_e), and tidal oscillatory salt transport due to temporal correlations between u and S (F_t). While salt outflux is mainly due to $-Q_f S_o$ (by freshwater discharge), salt influx is mainly due to F_e (by exchange flow) and F_t (by tidal pumping). For steady state, the outflux ($-Q_f S_o$) is balanced by the influx ($F_e + F_t$). Depending on the tidal energy and estuarine geometry, the relative importance of these two salt influx mechanisms varies.

The total salt influx ($F_e + F_t$) through the bay entrance was much larger than that across the Trinity Bay section (Fig. 9) even though the bay mouth is much narrower (2.5 km) compared to the Trinity Bay section (16 km). It is the difference in this total salt influx between the two sections that caused the spatially varying salinity recovery time (Fig. 8f). Except during the time under the direct impact of Harvey (i.e., between late August and early September), F_e was comparable between the two cross-sections, with a magnitude of 100–1000 kg salt s^{-1}. However, F_t was much larger, at least by one order of magnitude, at the bay entrance than at the Trinity Bay section (Table 2), largely owing to the larger tidal fluctuations in salinity and velocity. The salinity data show large tidal fluctuations near the bay entrance (Fig. 5c), and that the tidal fluctuations decreased upstream with virtually no tidal fluctuation in Trinity

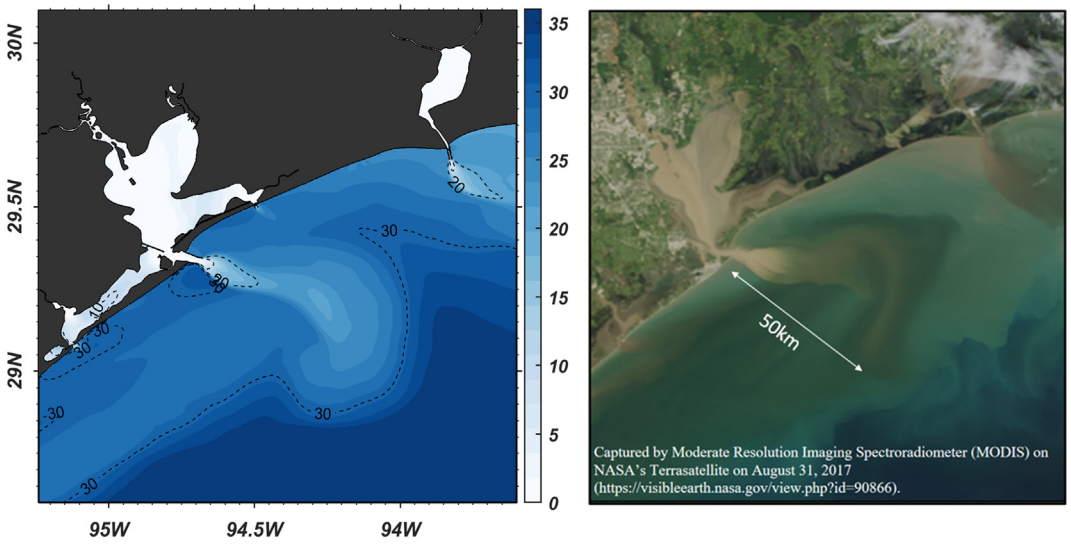

Fig. 7. Comparison of the modeled river plumes indicated by low salinity (a snapshot at 16:00 GMT on August 31, 2017) and the MODIS satellite image on August 31, 2017. Note that the overall shape, in terms of plume direction and offshore extent, is similar and that the model not only captures the plume from Galveston Bay but also that from Sabine Lake (in the upper-right corner).

Bay (Fig. 5a). Under normal conditions, i.e., from October to December, F_t was about 5–6 times larger than F_e at the bay entrance, indicating the dominant control of salt exchange from tidal pumping (Table 2). On the contrary, F_t and F_e were comparable at the Trinity Bay section, indicating a weak tidal exchange.

Both F_t and F_e showed great temporal variation at both cross-sections. At the bay entrance, both F_t and F_e increased drastically at the time of huge freshwater load (Fig. 9a and Table 2), which can be attributable to the increase in salinity gradient. The salinity inside the bay decreased quickly to zero during Harvey while the salinity on the shelf outside of the bay did not. Observational data show that the salinity on the shelf outside of Galveston Bay dropped from 32 to 16–20 psu during Harvey (Fig. 7 in Du et al., 2019a), whereas the salinity just inside the bay entrance dropped from 30 psu to 0 (Fig. 5c), resulting in a dramatic increase in salinity gradient. As the primary driving force for the exchange flow (MacCready and Geyer, 2010), increased salinity gradient enhances the exchange flow and thus F_e. Increased salinity gradient also causes a large fluctuation in salinity at the bay mouth between flood and ebb tides, enhancing the tidal pumping and thus F_t. The narrow outlet also helps tidal pumping. The tidal current through the narrow outlet is strong with a maximum speed of ~1 m s^{-1} despite the micro-tidal range (mean of 0.3 m), which leads to strong tidal pumping and thus F_t.

At the Trinity Bay section, on the other hand, there was no landward salt flux between late August and early September as the huge freshwater

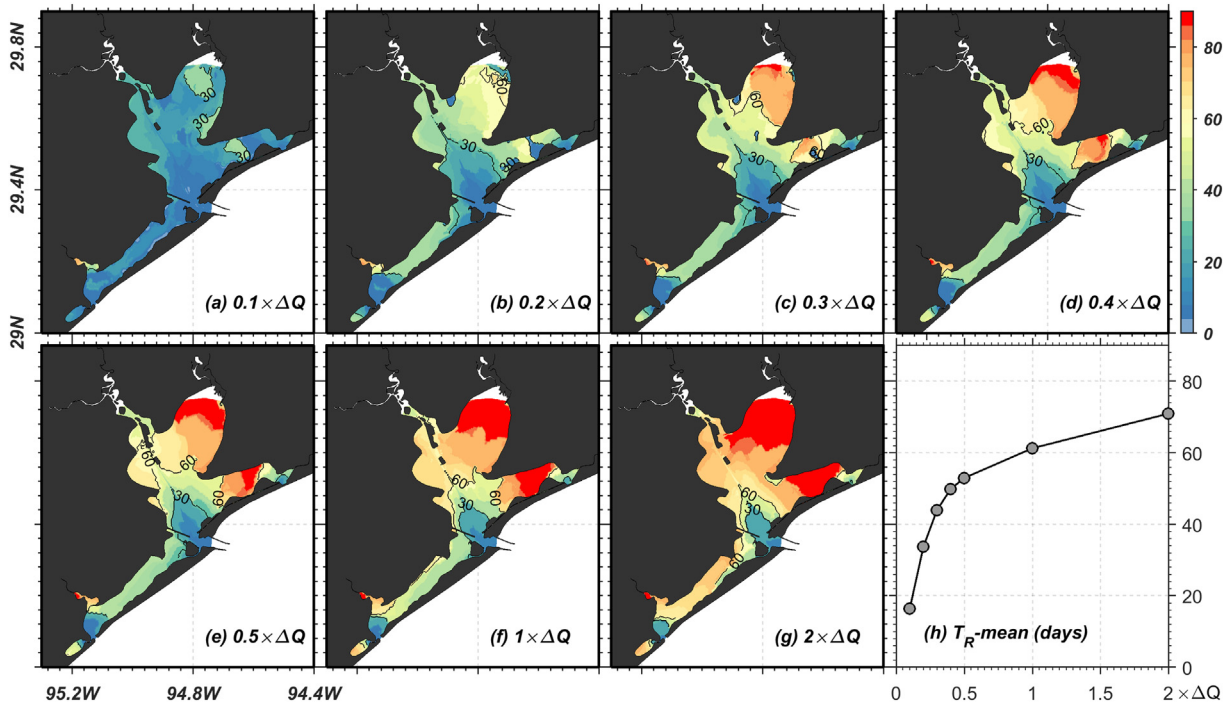

Fig. 8. Distribution of salinity recovery time (T_R) in days for different amounts of stormwater, i.e., 10%, 20%, 30%, 40%, 50%, 100% and 200% of the Harvey's stormwater ΔQ (a–g), and the variations in the bay-wide mean T_R as a function of stormwater (h). The blank areas in the upper bay indicate the region with salinity <5 psu even without the stormwater input for which T_R is not calculated.

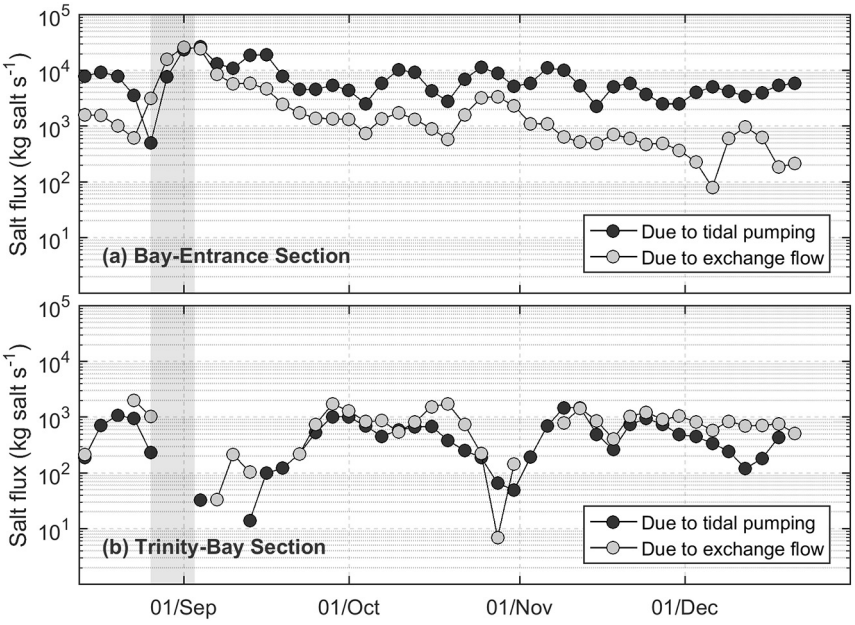

Fig. 9. Salt flux due to tidal pumping and exchange flow through the sections across the bay entrance (a) and the Trinity Bay (b), showing the samples at an interval of 3 days: see Fig. 4d for the locations of sections. The grey shades indicate the period of intense stormwater input from August 26 to September 3, 2017. Only the landward salt flux by tidal pumping or exchange flow is shown in (b), with the missing values indicating the seaward salt flux. Note the log scale for the y-axis, and that the orders of magnitude are very different between the two sections and between the two mechanisms of tidal pumping and exchange flow.

load pushed the bay water seaward (Fig. 9b). In addition, the salinity in the main bay (Fig. 5b) dropped to zero earlier than that in Trinity Bay (Fig. 5a), resulting in the reversed salinity gradient over a few days (Fig. 10). These two mechanisms combined to result in seaward flux of salt between late August and early September, i.e., during the time under the direct impact of the Harvey's stormwater. As the strong salt intrusion along the ship channel led to the normal salinity gradient (i.e., higher salinity in the main bay than in Trinity Bay), landward salt influx resumed after mid-September.

The shelf current also plays an important role for the strong tidal pumping at the bay entrance. Shelf transport is known to affect greatly the water exchange between ocean and estuary (Du and Shen, 2017; Zhang et al., 2019). Salinity snapshots on September 13–14, about two weeks after the stormwater release, show clearly how the shelf current facilitated the salt exchange (Fig. 11). Over a tidal cycle, the bay "breathed out" low salinity water during ebb. As the along-shelf current moved the bulb of low salinity water off the bay entrance, the bay "breathed in" new high salinity water during the following flood. This process helped maintain relatively high salinity gradient and enhanced the salt flux due to tidal pumping and exchange flow at the bay entrance. On the other hand, with no equivalent renewal process at the Trinity Bay section, water mass just moved back and forth over a tidal cycle, resulting in relatively small salinity gradient and salt flux between the main bay and the sub-bay, and leading to a long stalling of low salinity water (Fig. 5a) and thus long salinity recovery time (Fig. 8f). While the shelf current enhancing tidal pumping at the bay entrance, its influence depends on direction as well as strength. For instance, an upcoast shelf current is likely more effective than a downcoast shelf current in enhancing tidal pumping for Galveston Bay as a downcoast shelf current may reduce the salinity on Texas shelf by bringing low-freshwater from the Mississippi-Atchafalaya River system (Du et al., 2019b).

4.2. Implications of slow salinity recovery on estuarine ecosystem

Input of stormwater affects not only the hydrodynamic processes but also the processes related to water quality and estuarine ecosystem. The influence of stormwater can be short- or long-lasting, depending greatly on the recovery speed of physical conditions (e.g., salinity, temperature, and estuarine circulation), the exchange processes (e.g., nutrient exchange between estuary and ocean), as well as the resiliency of marine species to the exposure of freshwater (Conner et al., 1989; Greening et al., 2006; Paerl et al., 2006; Wetz and Paerl, 2008; Munroe et al., 2013; Tweedley et al., 2016). Many species in estuaries are sensitive to salinity level. For example, plankton community (both phyto- and zooplankton), fish, and marsh are typically distributed along the salinity gradient and grow better under a specific optimal salinity range. Long exposure to low salinity may lead to devastating mortality, particularly for benthic species that have limited mobility, e.g., oysters (Munroe et al., 2013).

The spatial variation of the salinity recovery time (Fig. 8f) appears to be consistent with the changes in the phytoplankton community in Galveston Bay during and after Harvey. The phytoplankton community in the lower bay was dominated by estuarine and marine species before Harvey, transitioned to primarily freshwater species immediately

Table 2
Salt flux contribution from tidal pumping and exchange flow at the bay entrance section and the Trinity Bay section. Average values for October–December reflect the normal conditions, while average values for August–September reflect conditions with stormwater.

Section	Contribution from	Salt flux (kg salt s^{-1}) averaged over		
		August–September	October–December	August–December
Bay entrance	Tidal pumping (F_t)	10,794	5693	7547
	Exchange flow (F_e)	6707	1002	3072
Trinity Bay	Tidal pumping (F_t)	306	515	438
	Exchange flow (F_e)	−232	770	405

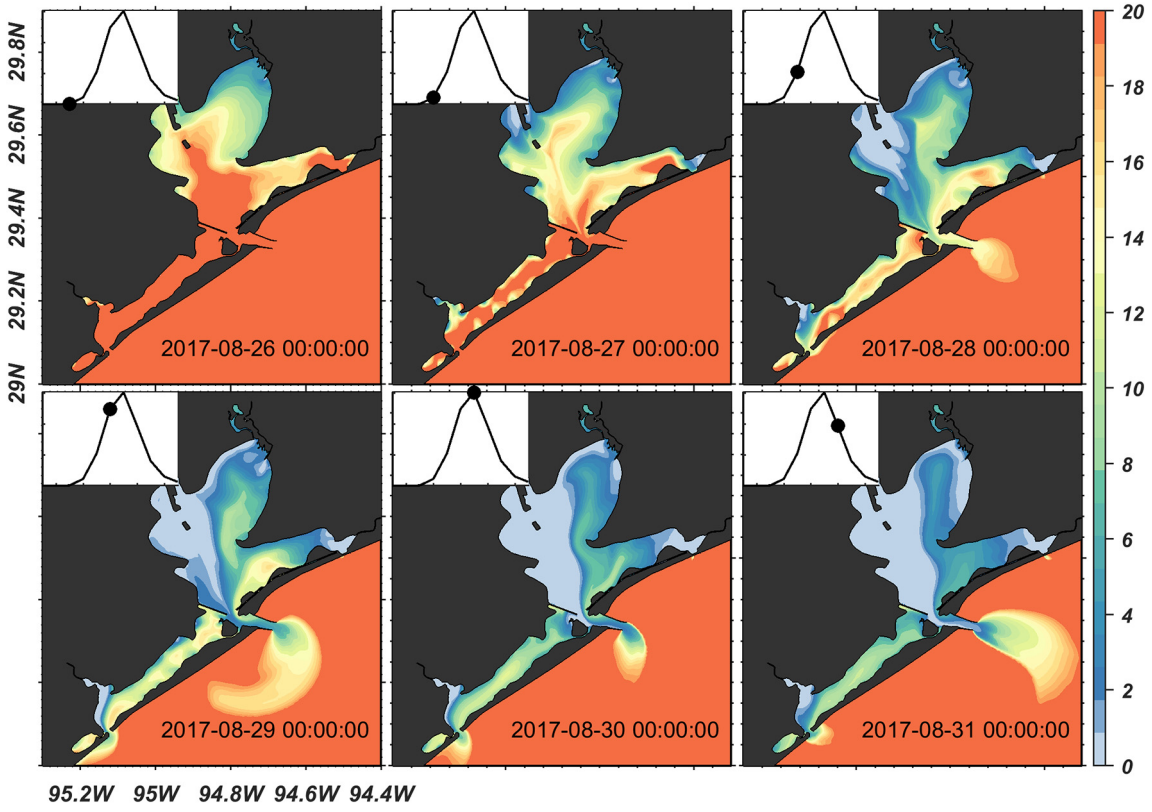

Fig. 10. Snapshots of salinity map before and during the release of the Harvey's stormwater, with the insets showing the corresponding time of the streamflow from San Jacinto River. Note the salinity difference between the main bay and Trinity Bay. Salinity in Trinity Bay was smaller compared to the main bay before the stormwater release. The salinity trend, however, was reversed during the stormwater release because of a faster decreasing of salinity in the main bay due to very large stormwater release from San Jacinto River, resulting in the reversed salinity gradient between the main bay and Trinity Bay.

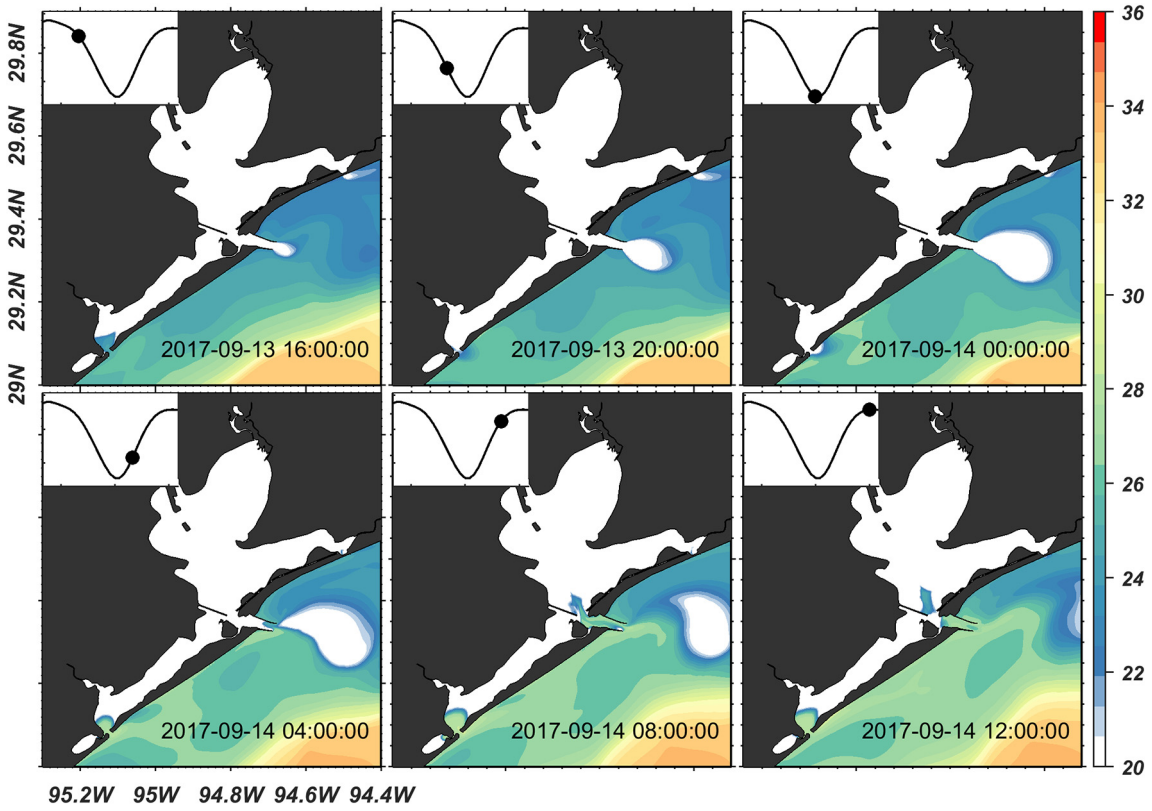

Fig. 11. Snapshots of salinity map with the insets showing the corresponding tidal phase. Note how the detachment of low salinity water on the shelf facilitates salt influx due to tidal pumping during the next flooding current.

following the flooding event, and back to marine phytoplankton similar to pre-Harvey conditions after one month following the storm (McAmis et al., 2018; Steichen et al., 2018; Liu et al., 2019). The recovery in the phytoplankton community was slower in the upper bay (J.L. Steichen, personal communication).

5. Conclusion

Extreme precipitation events are rare but likely to occur more frequently under the warming climate. This study takes the record-breaking precipitation event during Hurricane Harvey as an example to examine how the estuarine salinity recovers after a storm and discuss the underlying mechanisms for the spatially varying salinity recovery time. The salinity recovery time had a mean of two months over the entire Galveston Bay, but with great spatial variability. The spatial variability was explained by different contributions to salt influx from exchange flow and tidal pumping. Tidal pumping facilitated by the shelf current was the dominant mechanism for salt influx at the bay entrance, while the contributions from tidal pumping and exchange flow were comparable for salt influx to Trinity Bay. Numerical experiments reveal that the bay-wide mean salinity recovery time has a non-linear relationship with the stormwater input, with the rate of increase in the recovery time decreasing when stormwater input increases.

The spatial distribution of salinity recovery time and the underlying mechanisms are likely applicable for shallow estuaries with narrow outlets, which are common along the northern Gulf of Mexico, e.g., Apalachicola Bay, Mobile Bay, Matagorda Bay, Aransas Bay, and Corpus Christi Bay. The role of the shelf current for salinity recovery as identified by the present study shall also be applicable to other estuaries. The recovery time of salinity seems to be a useful timescale for the impact assessment of extreme precipitation events on estuarine systems. The present approach using a hydrodynamic model will be able to provide a relatively quick assessment of the environmental pressure of extreme events on target estuaries, highlighting the importance of validated hydrodynamic models that can reproduce both the normal and extreme conditions. The approach is not limited to extreme precipitation, but can also be applied to other extreme events such as severe drought and flood.

Supplementary data to this article can be found online at https://doi.org/10.1016/j.scitotenv.2019.03.265.

Acknowledgements

We like to acknowledge the TWDB (Texas Water Development Board), TABS (Texas Automated Buoy System), and USGS (U.S. Geological Survey) for the sources of the continuous monitoring data. We also like to acknowledge the Texas Coastal Management Program, the Texas General Land Office and NOAA for partial funding of this study through CMP Contract #19-040-000-B074. The numerical simulations were performed on the High-Performance Computing systems at College of William and Mary.

References

Balaguru, K., Foltz, G.R., Leung, L.R., 2018. Increasing magnitude of hurricane rapid intensification in the central and eastern tropical Atlantic. Geophys. Res. Lett. 45 (9), 4238–4247. https://doi.org/10.1029/2018GL077597.

Cardoso, P.G., Raffaelli, D., Lillebø, A.I., Verdelhos, T., Pardal, M.A., 2008. The impact of extreme flooding events and anthropogenic stressors on the macrobenthic communities' dynamics. Estuar. Coast. Shelf Sci. 76 (3), 553–565. https://doi.org/10.1016/j.ecss.2007.07.026.

Carrere, L., Lyard, F., Cancet, M., Guillot, A., 2015. FES 2014, a new tidal model on the global ocean with enhanced accuracy in shallow seas and in the Arctic region, In: Abstracts of the EGU General Assembly 2015. Vienna, Austria, April 12–17, 2015. http://adsabs.harvard.edu/abs/2015EGUGA..17.5481C.

Casas, S.M., Lavaud, R., La Peyre, M.K., Comeau, L.A., Filgueira, R., La Peyre, J.F., 2018. Quantifying salinity and season effects on eastern oyster clearance and oxygen consumption rates. Mar. Biol. 165, 90. https://doi.org/10.1007/s00227-018-3351-x.

Conner, W.H., Day Jr., J.W., Baumann, R.H., Randall, J.M., 1989. Influence of hurricanes on coastal ecosystems along the northern Gulf of Mexico. Wetl. Ecol. Manag. 1 (1), 45–56. https://doi.org/10.1007/BF00177889.

Donat, M.G., Lowry, A.L., Alexander, L.V., O'Gorman, P.A., Maher, N., 2016. More extreme precipitation in the world's dry and wet regions. Nat. Clim. Chang. 6 (5), 508–513. https://doi.org/10.1038/nclimate2941.

Du, J., Shen, J., 2017. Transport of riverine material from multiple rivers in the Chesapeake Bay: important control of estuarine circulation on the material distribution. J. Geophys. Res. Biogeo. 122 (11), 2998–3113. https://doi.org/10.1002/2016JG003707.

Du, J., Shen, J., Zhang, Y.J., Ye, F., Liu, Z., Wang, Z., Wang, Y.P., Yu, X., Sisson, M., Wang, H.V., 2018a. Tidal response to sea-level rise in different types of estuaries: the importance of length, bathymetry, and geometry. Geophys. Res. Lett. 45 (1), 227–235. https://doi.org/10.1002/2017GL075963.

Du, J., Park, K., Shen, J., Dzwonkowski, B., Yu, X., Yoon, B.I., 2018b. Role of baroclinic processes on flushing characteristics in a highly stratified estuarine system, Mobile Bay, Alabama. J. Geophys. Res. Oceans 123 (7), 4518–4537. https://doi.org/10.1029/2018JC013855.

Du, J., Park, K., Dellapenna, T.M., Clay, J.M., 2019a. Dramatic hydrodynamic and sedimentary responses in Galveston Bay and adjacent inner shelf to Hurricane Harvey. Sci. Total Environ. 653, 554–564. https://doi.org/10.1016/J.SCITOTENV.2018.10.403.

Du, J., Park, K., Shen, J., Zhang, Y.J., Yu, X., Ye, F., Wang, Z., Rabalais, N.N., 2019b. A hydrodynamic model for Galveston Bay and the shelf in the northwestern Gulf of Mexico. Ocean Sci. Discuss. https://doi.org/10.5194/os-2019-9 in review.

Emanuel, K., 2017. Assessing the present and future probability of Hurricane Harvey's rainfall. P. Natl. A. Sci. USA. 114 (48), 12681–12684. https://doi.org/10.1073/pnas.1716222114.

Frazer, T.K., Notestein, S.K., Jacoby, C.A., Littles, C.J., Keller, S.R., Swett, R.A., 2006. Effects of storm-induced salinity changes on submersed aquatic vegetation in Kings Bay. Florida. Estuar. Coast. 29 (6A), 943–953. https://doi.org/10.1007/bf02798655.

Fritz, A., Samenow, J., 2017. Harvey Unloaded 33 Trillion Gallons of Water in the U.S. https://www.washingtonpost.com/news/capital-weather-gang/wp/2017/08/30/harvey-has-unloaded-24-5-trillion-gallons-of-water-on-texas-and-louisiana/?utm_term=.92eae8c1e7da, Accessed date: 10 March 2019.

Gong, W., Shen, J., Reay, W.G., 2007. The hydrodynamic response of the York River estuary to Tropical Cyclone Isabel, 2003. Estuar. Coast. Shelf S. 73 (3–4), 695–710. https://doi.org/10.1016/j.ecss.2007.03.012.

Greening, H., Doering, P., Corbett, C., 2006. Hurricane impacts on coastal ecosystems. Estuar. Coast. 29 (6), 877–879. https://doi.org/10.1007/BF02798646.

Hagy, J.D., Lehrter, J.C., Murrell, M.C., 2006. Effects of hurricane Ivan on water quality in Pensacola Bay. Florida. Estuar. Coast. 29 (6A), 919–925. https://doi.org/10.1007/BF02798651.

Huzzey, L.M., Brubaker, J.M., 1988. The formation of longitudinal fronts in a coastal plain estuary. J. Geophys. Res. 93 (C2), 1329–1334. https://doi.org/10.1029/JC093iC02p01329.

Kantha, L.H., Clayson, C.A., 1994. An improved mixed layer model for geophysical applications. J. Geophys. Res. 99 (C12), 25235–25266. https://doi.org/10.1029/94JC02257.

Knapp, A.K., Beier, C., Briske, D.D., Classen, A.T., Luo, Y., Reichstein, M., Smith, M.D., Smith, S.D., Bell, J.E., Fay, P.A., Heisler, J.L., Leavitt, S.W., Sherry, R., Smith, B., Weng, E., 2008. Consequences of more extreme precipitation regimes for terrestrial ecosystems. BioScience 58 (9), 811–821. https://doi.org/10.1641/B580908.

Knight, D.B., Davis, R.E., 2009. Contribution of tropical cyclones to extreme rainfall events in the southeastern United States. J. Geophys. Res. Atmos. 114, D23102. https://doi.org/10.1029/2009JD012511.

Lerczak, J.A., Geyer, W.R., 2004. Modeling the lateral circulation in straight, stratified estuaries. J. Phys. Oceanogr. 34 (6), 1410–1428. https://doi.org/10.1175/1520-0485(2004)034<1410:MTLCIS>2.0.CO;2.

Lerczak, J.A., Geyer, W.R., Chant, R.J., 2006. Mechanisms driving the time-dependent salt flux in a partially stratified estuary. J. Phys. Oceanogr. 36 (12), 2296–2311. https://doi.org/10.1175/JPO2959.1.

Li, M., Zhong, L., Boicourt, W.C., Zhang, S., Zhang, D.-L., 2006. Hurricane-induced storm surges, currents and destratification in a semi-enclosed bay. Geophys. Res. Lett. 33 (2), L02604. https://doi.org/10.1029/2005GL024992.

Liu, B., D'Sa, E.J., Joshi, I.D., 2019. Floodwater impact on Galveston Bay phytoplankton taxonomy, pigment composition and photo-physiological state following Hurricane Harvey from field and ocean color (Sentinel-3A OLCI) observations. Biogeosci. Discuss. https://doi.org/10.5194/bg-2018-504 in review.

MacCready, P., Geyer, W.R., 2010. Advances in estuarine physics. Annu. Rev. Mar. Sci. 2, 35–58. https://doi.org/10.1146/annurev-marine-120308-081015.

McAmis, A. K., Steichen, J. L., Quigg, A., 2018. The effects of Hurricane Harvey on the phytoplankton community in Galveston Bay. In: Abstracts of the 2018 GERS Meeting: Ecosystem Resilience and Restoration in a Changing World, Galveston, Texas, November 8–10, 2018.

Milliner, C., Materna, K., Bürgmann, R., Fu, Y., Moore, A.W., Bekaert, D., Adhikari, S., Argus, D.F., 2018. Tracking the weight of Hurricane Harvey's stormwater using GPS data. Sci. Adv. 4 (9), eaau2477. https://doi.org/10.1126/sciadv.aau2477.

Moriasi, D.N., Arnold, J.G., Van Liew, M.W., Bingner, R.L., Harmel, R.D., Veith, T.L., 2007. Model evaluation guidelines for systematic quantification of accuracy in watershed simulations. T. ASABE 50, 885–900. https://doi.org/10.1016/j.jhydrol.2012.12.004.

Munroe, D., Tabatabai, A., Burt, I., Bushek, D., Powell, E.N., Wilkin, J., 2013. Oyster mortality in Delaware Bay: impacts and recovery from Hurricane Irene and Tropical Storm Lee. Estuar. Coast. Shelf Sci. 135, 209–219. https://doi.org/10.1016/j.ecss.2013.10.011.

Nash, J.E., Sutcliffe, J.V., 1970. River flow forecasting through conceptual models, part I - a discussion of principles. J. Hydrol. 10 (3), 282–290. https://doi.org/10.1016/0022-1694(70)90255-6.

Paerl, H.W., Valdes, L.M., Joyner, A.R., Peierls, B.L., Piehler, M.F., Riggs, S.R., Christian, R.R., Eby, L.A., Crowder, L.B., Ramus, J.S., Clesceri, E.J., Buzzelli, C.P., Luettich Jr., R.A., 2006. Ecological response to hurricane events in the Pamlico Sound system, North Carolina,

and implications for assessment and management in a regime of increased frequency. Estuar. Coast. 29 (6), 1033–1045. https://doi.org/10.1007/BF02798666.
Peierls, B.L., Christian, R.R., Paerl, H.W., 2003. Water quality and phytoplankton as indicators of hurricane impacts on a large estuarine ecosystem. Estuaries 26 (5), 1329–1343. https://doi.org/10.1007/BF02803635.
Pfahl, S., O'Gorman, P.A., Fischer, E.M., 2017. Understanding the regional pattern of projected future changes in extreme precipitation. Nat. Clim. Chang. 7 (6), 423–427. https://doi.org/10.1038/nclimate3287.
Posey, M., Lindberg, W., Alphin, T., Vose, F., 1996. Influence of storm disturbance on an offshore benthic community. B. Mar. Sci. 59 (3), 523–529.
Rego, J.L., Li, C., 2010. Storm surge propagation in Galveston Bay during Hurricane Ike. J. Mar. Sys. 82 (4), 265–279. https://doi.org/10.1016/j.jmarsys.2010.06.001.
Ritter, A., Muñoz-Carpena, R., 2013. Performance evaluation of hydrological models: statistical significance for reducing subjectivity in goodness-of-fit assessments. J. Hydrol. 480, 33–45. https://doi.org/10.1016/j.jhydrol.2012.12.004.
Scheffer, M., Carpenter, S., Foley, J.A., Folke, C., Walker, B., 2001. Catastrophic shifts in ecosystems. Nature 413, 591–596.
Sebastian, A., Proft, J., Dietrich, J.C., Du, W., Bedient, P.B., Dawson, C.N., 2014. Characterizing hurricane storm surge behavior in Galveston Bay using the SWAN+ADCIRC model. Coast. Eng. 88, 171–181. https://doi.org/10.1016/j.coastaleng.2014.03.002.
Shen, J., Wang, H., Sisson, M., Gong, W., 2006. Storm tide simulation in the Chesapeake Bay using an unstructured grid model. Estuar. Coast. Shelf Sci. 68 (1–2), 1–16. https://doi.org/10.1016/j.ecss.2005.12.018.
Steichen, J. L., Windham, R., Hala, D., Kaiser, K., Labonté, J. M., Petersen, L. H., Bacosa, H., Bretherton, L., Kamalanathan, M., Setta, S., Quigg, A., 2018. Rapid physicochemical and biological assessment of Galveston Bay in the wake of Hurricane Harvey. In: Abstracts of the 2018 Ocean Sciences Meeting, AGU, Portland, Oregon, February 11–16, 2018.
Tweedley, J.R., Hallettt, C.S., Warwick, R.M., Clarke, K.R., Potter, I.C., 2016. The hypoxia that developed in a microtidal estuary following an extreme storm produced dramatic changes in the benthos. Mar. Freshw. Res. 67 (3), 327–341. https://doi.org/10.1071/MF14216.
Umlauf, L., Burchard, H., 2003. A generic length-scale equation for geophysical turbulence models. J. Mar. Res. 61 (2), 235–265. https://doi.org/10.1357/002224003322005087.
Valle-Levinson, A., Wong, K.-C., Bosley, K.T., 2002. Response of the lower Chesapeake Bay to forcing from Hurricane Floyd. Cont. Shelf Res. 22 (11−13), 1715–1729. https://doi.org/10.1016/S0278-4343(02)00034-1.
van Oldenborgh, G. J., van der Wiel, K., Sebastian, A., Singh, R., Arrighi, J., Otto, F., Haustein, K., Li, S., Vecchi, G., Cullen, H., 2018. Corrigendum: Attribution of extreme rainfall from Hurricane Harvey, August 2017. Environ. Res. Lett. 13, 019501. doi:https://doi.org/10.1088/1748-9326/aaa343.
Walker, N.D., 2001. Tropical storm and hurricane wind effects on water level, salinity, and sediment transport in the river-influenced Atchafalaya-Vermilion Bay System, Louisiana, USA. Estuaries 24 (4), 498–508. https://doi.org/10.2307/1353252.
Wetz, M.S., Paerl, H.W., 2008. Estuarine phytoplankton responses to hurricanes and tropical storms with different characteristics (trajectory, rainfall, winds). Estuar. Coast. 31 (2), 419–429. https://doi.org/10.1007/s12237-008-9034-y.
Weyhenmeyer, G.A., Willén, E., Sonesten, L., 2004. Effects of an extreme precipitation event on water chemistry and phytoplankton in the Swedish Lake Mälaren. Boreal Environ. Res. 9 (5), 409–420.
Willmott, C.J., 1981. On the validation of models. Phys. Geogr. 2 (2), 184–194. https://doi.org/10.1080/02723646.1981.10642213.
Ye, F., Zhang, Y.J., Wang, H.V., Friedrichs, M.A.M., Irby, I.D., Alteljevich, E., Valle-Levinson, A., Wang, Z., Huang, H., Shen, J., Du, J., 2018. A 3D unstructured-grid model for Chesapeake Bay: importance of bathymetry. Ocean Model 127, 16–39. https://doi.org/10.1016/j.ocemod.2018.05.002.
Zhang, Y., Baptista, A.M., 2008. SELFE: A semi-implicit Eulerian-Lagrangian finite-element model for cross-scale ocean circulation. Ocean Model 21 (3–4), 71–96. https://doi.org/10.1016/j.ocemod.2007.11.005.
Zhang, Q., Brady, D.C., Ball, W.P., 2013. Long-term seasonal trends of nitrogen, phosphorus, and suspended sediment load from the non-tidal Susquehanna River Basin to Chesapeake Bay. Sci. Total Environ. 452-453, 208–221. https://doi.org/10.1016/j.scitotenv.2013.02.012.
Zhang, Y.J., Ateljevich, E., Yu, H.C., Wu, C.H., Yu, J.C.S., 2015. A new vertical coordinate system for a 3D unstructured-grid model. Ocean Model 85, 16–31. https://doi.org/10.1016/j.ocemod.2014.10.003.
Zhang, Y.J., Ye, F., Stanev, E.V., Grashorn, S., 2016. Seamless cross-scale modeling with SCHISM. Ocean Model 102, 64–81. https://doi.org/10.1016/j.ocemod.2016.05.002.
Zhang, H., Cheng, W., Chen, Y., Shi, Z., Gong, W., Liu, S., 2019. Importance of large-scale coastal circulation on bay-shelf exchange and residence time in a subtropical embayment, the northern South China Sea. Ocean Coast. Manage. 168, 72–89. https://doi.org/10.1016/j.ocecoaman.2018.10.033.